

ANALYSIS OF A DUAL AIR DATA AND MULTI-HOLE PRESSURE PROBE BOOM

Darren T. Rajeepan[1], Nicholas J. Lawson[1] & Andras Galffy[2]

[1]School of Aerospace, Mechanical and Mechatronics Engineering, The University of Sydney, Camperdown, NSW 2006, Australia
[2]Turbulence Solutions, Wollzeile 1-3/3.2, 1010 Wien, Austria

Abstract

This paper presents the integration of a dual air data and multi-hole pressure probe boom and the upgrade of its data acquisition system. A WindShape gust tunnel was used to conduct a series of static flowfield measurement tests to measure angle of attack (α) and airspeed (v). These results and their relative errors (ε_α) are presented alongside the correlation between the recorded turbulence intensity (I) and ε_α. The results from a frequency analysis are also presented. Sources of error and considerations for future experiments are discussed and the foundation for future work is also presented.

Keywords: Aerodynamics, turbulence suppression, gust tunnel

1. Introduction

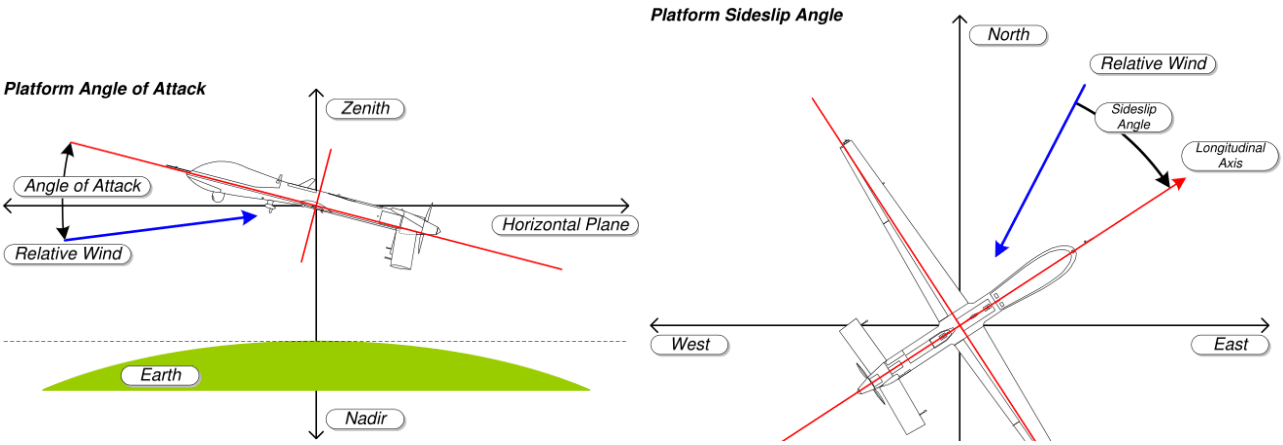
This section will outline the motivation and context for the development of a turbulence suppression system as well as the specific aims and objectives of this paper.

Turbulence is one of the leading causes of in-flight injuries and remains a threat to the safe operation of aircraft worldwide. In May of 2024, a Boeing 777-300ER encountered severe turbulence over Myanmar resulting in injuries to 140 passengers and 1 fatality from a heart failure. [1] Turbulence Suppression systems involve the measurement of velocity components directly ahead of the aircraft. This data can then be used to predict changes to aircraft attitude angles (angle of attack α [2] and sideslip angle β [3]) and, using a feedforward controller, can actuate control surfaces to counter these changes [4]. Accurately capturing flowfield information whilst accounting for time lag and other sources of error, as well as measuring real-time α and β are critical to the development of such systems. The University of Sydney has a Jabiru J400 with registration VH-USY used for flight testing purposes as well as a SpaceAge Control (SAC) data probe designed for use on the aircraft. These can be used in the development of a turbulence suppression system.

As part of the development of a complete turbulence suppression system, the objectives of this project included the modernisation of the data acquisition system of the SAC probe through the integration of the UEI PowerDNA cube. It also involved the integration of a Turbulence Solutions (TS) 4-hole probe. Using this setup, the aim was then to conduct a series of static tests using a WindShape gust tunnel to obtain α, β and v data. Analysis on results would help show the effectiveness of the overall system in recording flowfield measurements, accounting for errors such as time lag and creating a foundation for further tests to aid in the development of a turbulence suppression system.

2. Literature Review

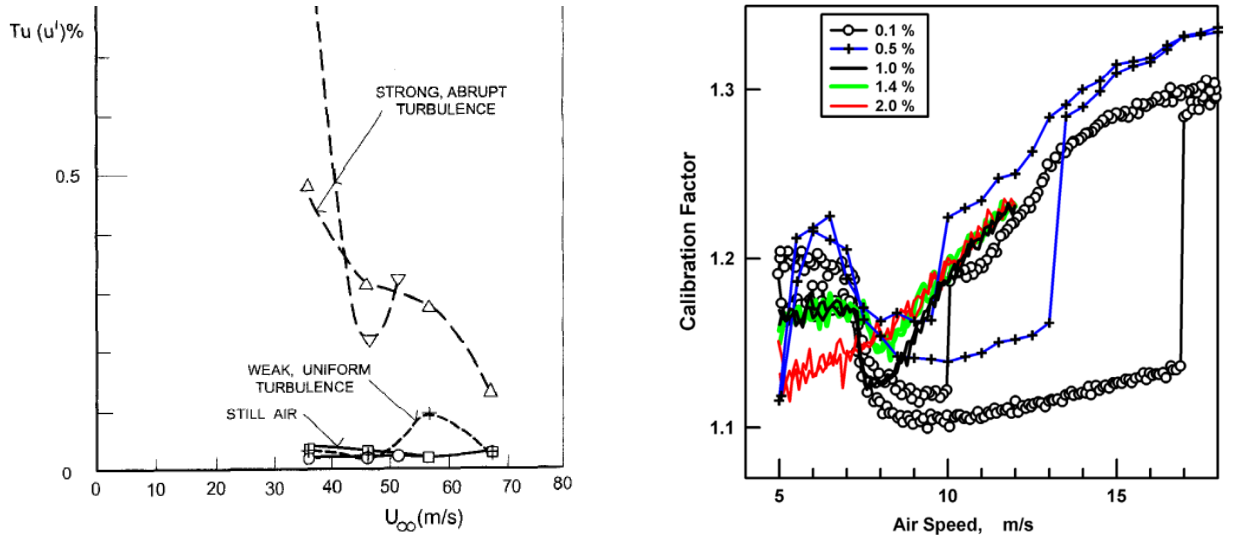
Aircraft attitude angles are critical considerations for flight. Angle of attack α is defined as the relative angle between the oncoming freestream and the aircraft's chord line [2] and is shown in Figure 1a. Sideslip angle β is defined as the relative angle between the aircraft's heading and actual track [3] and is shown in Figure 1b.



(a) Angle of Attack α (b) Sideslip Angle β

Figure 1 – Aircraft Attitude Angles (Source: Motion Imagery Standards Board)

An important consideration for flowfield experiments that will be highlighted by this paper is that of Turbulence Intensity (I) and its impact on probe calibration. I is defined as the root mean squared fluctuation of recorded velocities over the mean velocity for a given dataset. Figure 2a show I values recorded in-flight from an experiment conducted in 1998 on an LFU 205 by DLR. This is an aircraft of relatively similar performance parameters to the J400 and shows that for an airspeed range of $36ms^{-1} < U_\infty < 70ms^{-1}$, a range of $0.04\% < I < 1.0\%$ was recorded. Figure 2b show the results for an experiment conducted in 2013 by the NIST. They show a variation in the required calibration factor of up to 10% for a range of $0.1\% < I < 2\%$. This highlights the importance of correctly calibrating multi-hole probes for a given I value and ensuring velocity variations are minimised during experiments to minimise errors.



(a) In-flight *I* values measured [5] (b) Probe calibration factor variation for changing *I* [6]

Figure 2 – Influence of Turbulence Intensity

3. Methodology

This section will outline the experimental setup used to obtain flowfield information including the data processing methods and error analysis which is outlined.

The experimental setup comprises of a SAC probe designed for a Jabiru J400 mounted on a twin-tripod setup. This probe consists of an α vane and a β vane. An aerofoil mount allows for the TS 4-hole probe to be integrated into the setup. It should be noted that the 'Wall Effect' consideration of the minimum distance between an air data probe and the wall of a wind tunnel was used as a conservative measure to minimise interference between the two probes and to determine the dimensions of the aerofoil mount. [7] Both probes are normally capable of recording angle of attack, sideslip angle and airspeed values. The pressure transducers in the SAC probe were deemed inoperative and this paper will only present α results as well as v recordings. Figures 3 and 4 show a photograph and schematic of the setup.

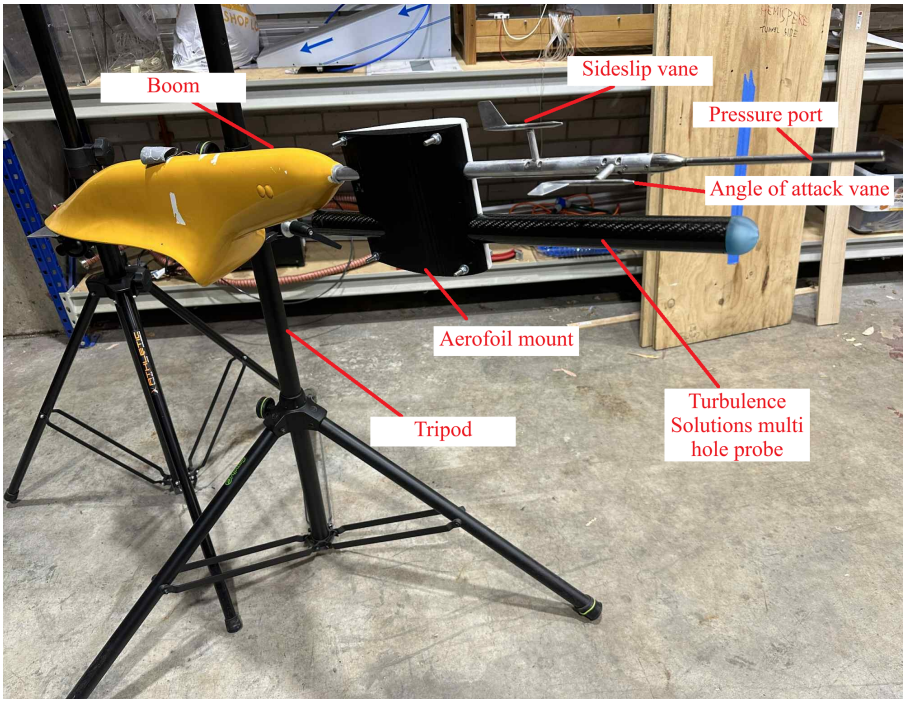


Figure 3 – Dual probe setup

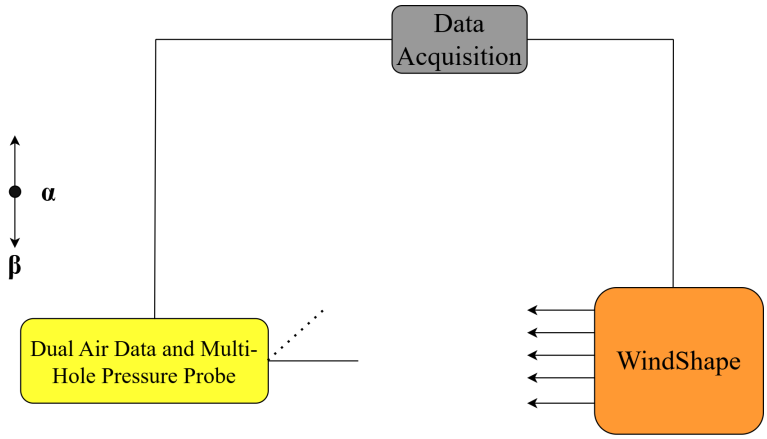
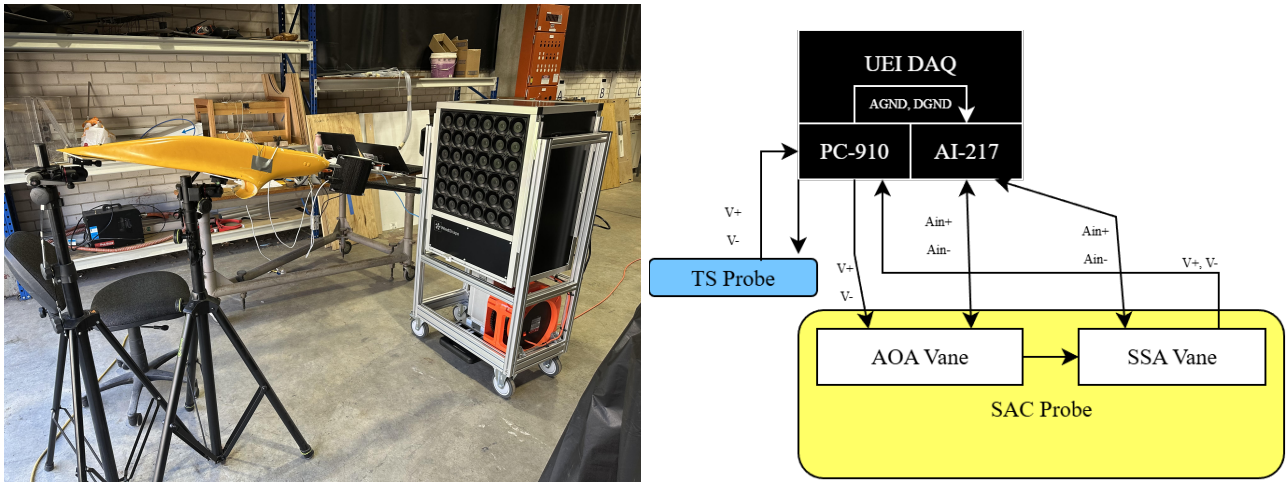


Figure 4 – Schematic of setup

A WindShape gust tunnel was used to provide airflow for this experiment. It is capable of providing a spatial and temporal profile varied to simulate gusts and turbulence. Figure 5a shows the WindShape

used for this experiment. A UEI PowerDNA cube was used for data acquisition from the SpaceAge Control probe, which was done with an AI-217 A/D board. [8] A PC-910 power conversion board in the cube was used for power supply to both probes. [9] Figure 5b illustrates the wiring schematic of this experiment.



(a) WindShape Gust Tunnel and Testing Setup

(b) Wiring Schematic

Figure 5 – Additional figures of experimental setup

Basic frequency analysis was conducted on some of the data collected to try and identify a series of phenomena including resonant frequencies of the boom and vortex shedding. The Discrete Fourier Transform (DFT) involves the decomposition of a signal into a series of sine and cosine waves and is calculated using Equations 1 and 2 below.

$$FT(x_n) = \sum_{n=0}^{N-1} x_n e^{\left(-\frac{2\pi nk}{N} i\right)} \tag{1}$$

$$c_k[i] = \cos\frac{2\pi k_i}{N}, \quad s_k[i] = \sin\frac{2\pi k_i}{N} \tag{2}$$

A Power Spectral Density (PSD) shows the relative energy from every signal frequency from the Fourier Transform by considering square magnitudes of spectral coefficients from the DFT process. The equation for the one-sided PSD is shown in Equation 3 below. [10]

$$G_k = G(f = f_k) = \frac{2}{Nf_s} X_k^* X_k = \frac{2}{N^2 \Delta f_s} X_k^* X_k \tag{3}$$

To determine if von Karman vortex shedding would be present in this experiment, a conservative estimate for the highest Reynolds Number (Re) for this experiment was determined as per below in Equation 4. This conservative estimate uses the maximum velocity of the flow from the WindShape and the widest diameter of the boom body from which vortices could be shed. As can be seen, the resulting Re is below the 2×10^5 sub-critical limit for von Karman vortex shedding. [11]

$$Re_{max} = \frac{u \cdot L}{\nu} = \frac{17.5 \times 0.1}{1.46 \times 10^{-5}} = 119,863 \tag{4}$$

The formula for calculating St is shown in Equation 5 below. A value of $St = 0.25$ was selected for the phenomena of von Karman vortex shedding. This value was chosen from a cylinder in the Ludweig tube experiment from Springer [10] and a 1986 NASA paper showing the validity of using a two dimensional cylinder analogy for vortex shedding and flow over a body similar to the dual air data probe of this experiment.[12]. The sample frequency of the UEI cube was unable to be fixed due to a technical issue and so to circumvent this, the sample frequency of each test run was printed alongside the raw voltage logs. Figure 6 shows the raw data results for a typical test case. It should be noted that test cases recorded sampling frequencies in the range of $2000Hz < f < 4000Hz$ ensuring

the Nyquist criteria was satisfied for identifying vortex shedding. Additionally, it should be noted that the duration of each data recording was adjusted such that 180,000 samples would be taken on each run.

$$St = \frac{fL}{U} = 0.25 \rightarrow 12.5Hz < f_{vK} < 43.5Hz \tag{5}$$

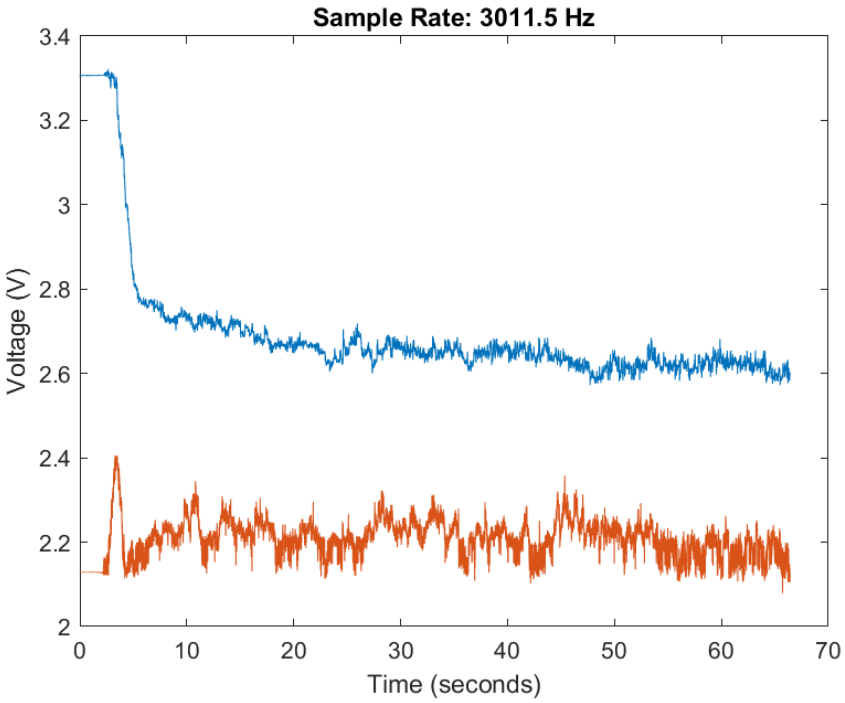


Figure 6 – Typical raw data log

I is defined as the RMS fluctuation of recorded velocities over the mean velocity value for a given dataset. Equation 6 below shows the u component of the Reynolds Averaging formula and Equation 7 shows the calculation of the I. Note that for this paper, only the u component will be considered.

$$u' = u - \bar{u} \tag{6}$$

$$I_u = \frac{u'}{V} \tag{7}$$

Relative error for α values was calculated using Equation 8 below. Note that the range of the α measurements of 30° was used rather than the recorded α value to ensure consistency across the range of values tested.

$$\varepsilon_\alpha = \frac{\alpha_{SAC} - \alpha}{30^\circ} \tag{8}$$

Equation 9 below was used to calculate the propagation of uncertainty in α results. Quantifiable sources of uncertainty considered included the IP65 Spirit Level only measuring to the closest 0.05° and a linearity error of $\pm 0.5\%$ of the transducers used in the SAC probe. The Bosch GLL 3-80 cross-line laser level used for setting the position of the WindShape had a cited uncertainty of $\pm 0.3mm/m$ [13] and was also considered. Calibration tape was laid out on the ground along the line projected by the laser line and an uncertainty value of $\pm 3mm$ was considered as well.

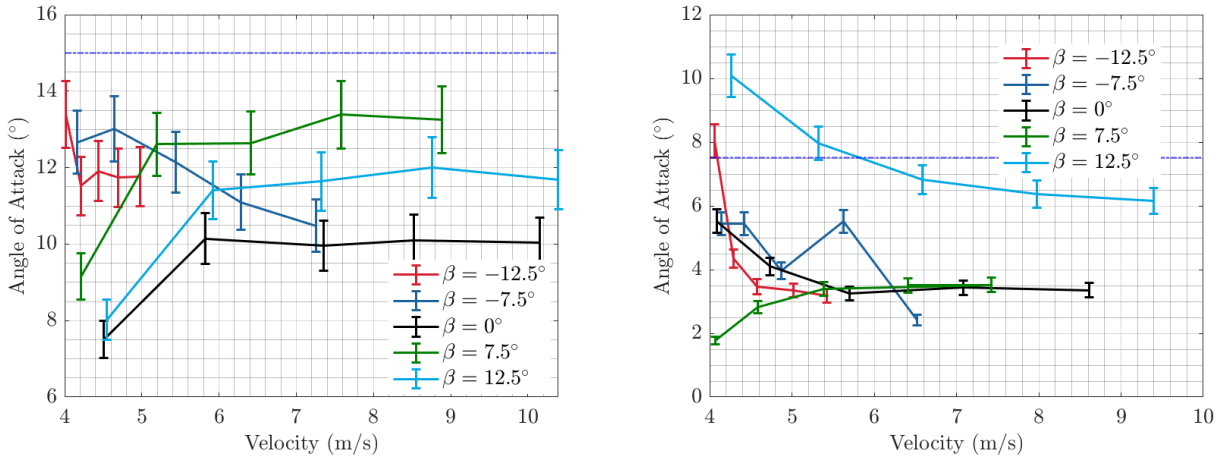
$$\frac{\sigma(\alpha)}{\alpha} = \sqrt{\left(\frac{\sigma(x_1)}{x_1}\right)^2 + \left(\frac{\sigma(x_2)}{x_2}\right)^2 + \ldots + \left(\frac{\sigma(x_n)}{x_n}\right)^2} \tag{9}$$

4. Results and Discussion

This section will outline the results obtained from this experiment. Section 4.1 will outline the α results obtained and cite sources of errors and inaccuracies with this experimental setup. Section 4.2 will outline the I values of this experiment and its correlation with relative error ε. Section 4.3 will outline the results of the frequency analysis conducted on this experiment.

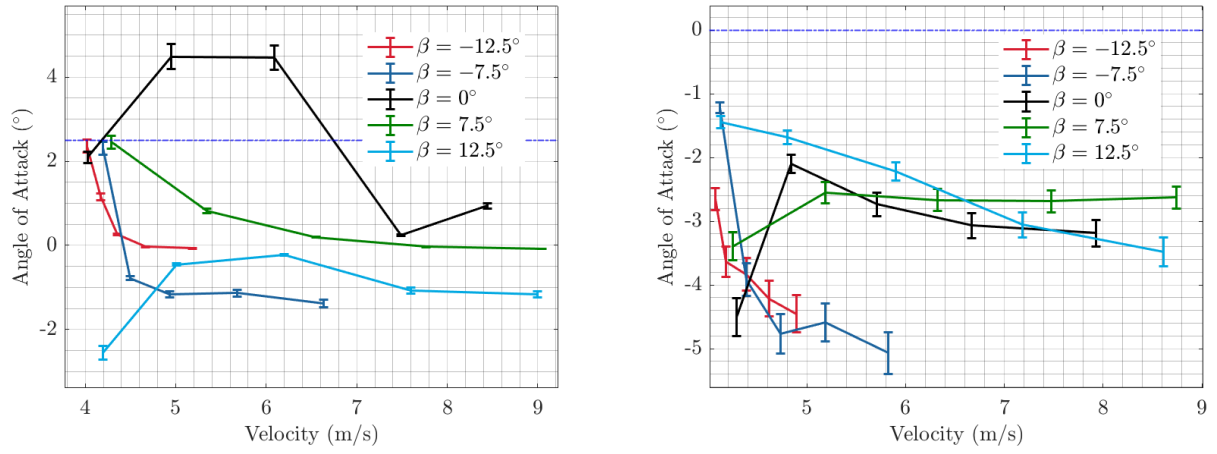
4.1 Angle of Attack Sweep

Figure 7, 8, 9 and 10 illustrates the recorded angle of attack values recorded by the SAC probe at five power settings for the WindShape tunnel and a series of five different sideslip settings. Table 1 shows the relative errors of these results, which range from $0\% < \varepsilon_\alpha < 25\%$.



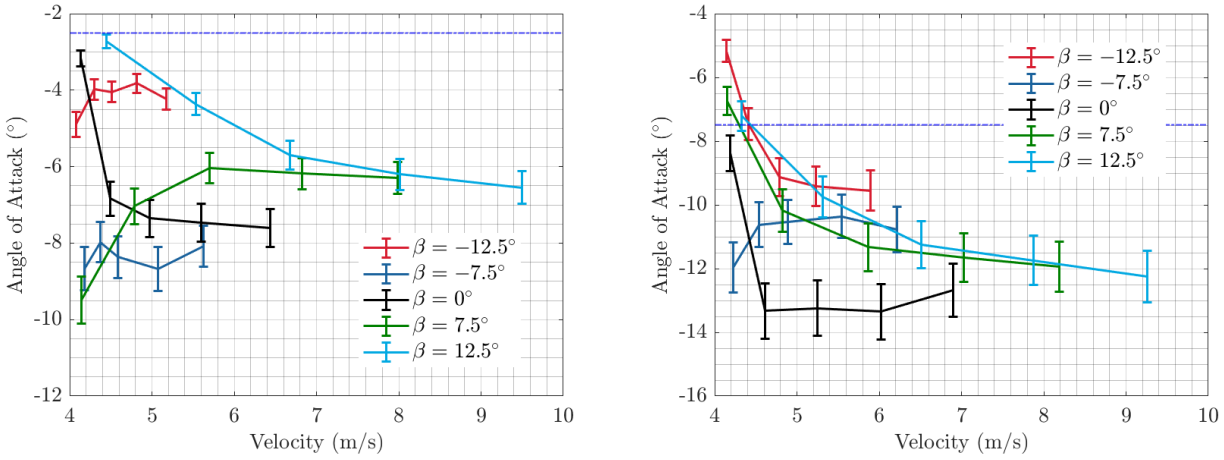
(a) $\alpha = 15°$ (b) $\alpha = 7.5°$

Figure 7 – α results



(a) $\alpha = 2.5°$ (b) $\alpha = 0°$

Figure 8 – α results



(a) $\alpha = -2.5°$ (b) $\alpha = -7.5°$

Figure 9 – α results

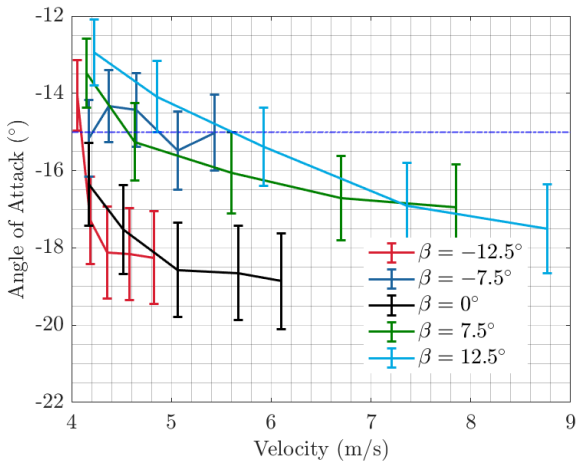


Figure 10 – α results $\alpha = -15°$

Table 1 – Range of ε_α values

α Setting (°)	-15	-7.5	-2.5	0	2.5	7.5	15
Maximum ε_α (%)	12.5	19.2	23.3	16.7	16.7	19.0	25.0
Minimum ε_α (%)	0	0	0.83	4.0	0	1.7	5.0

Likely sources of the variation in ε_α include the manual adjustment of the tripod height and position for each test run. This would have affected the precision of the position of the experimental setup with an estimated error impact of $\pm 6.5\%$. This value was estimated using uncertainty considerations outlined in Section 3. as well as from the calibration process. The calibration of the voltage reading to an angle was done using the same IP65 spirit level. This was held by hand to take measurements and this likely resulted in random errors from hand movements and shaking. Using a calibrated traverse instead, would have accounted for this and also enabled dynamic testing.

4.2 Turbulence Intensity Results

Initial observations of results from the TS probe showed very high ε_α ranging from $0.5\% < \varepsilon_\alpha < 206\%$. A correlation between Turbulence Intensity I and ε_α in the results from the TS probe was hypothesised due to the precise position of the probe not being controlled and it being in different sections of the open jet geometric profile of the WindShape. This would have resulted in high levels

of velocity variations and subsequently high I values. The strong impact of I outlined in literature [6] shows the importance of accounting for high I values when calibrating probes directly impacting the accuracy of results obtained. Figure 11 below show the I vs ε_α results obtained from the results and show a positive correlation between the two with respective ranges of $0.5\% < \varepsilon_\alpha < 206\%$ and $6.1\% < I < 16.9\%$.

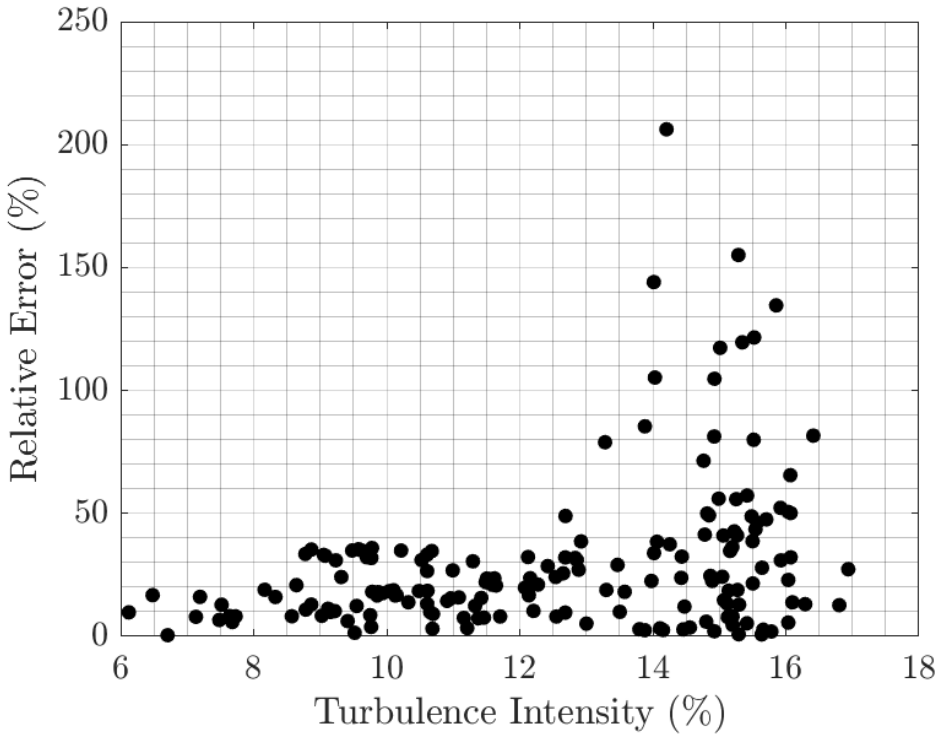
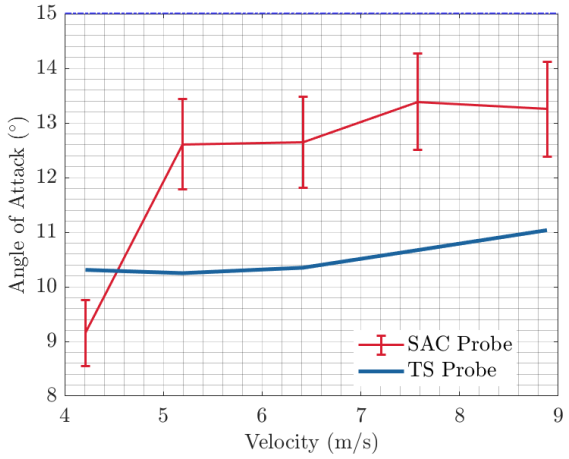
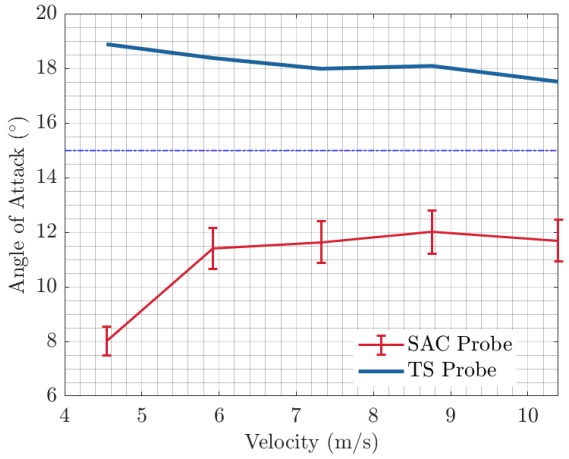


Figure 11 – Turbulence Intensity I vs Relative Error ε

This hypothesis appears likely when observing TS probe α results. Figures 12a and 12b show the TS probe results for test runs with relatively low I values with relative error range of $8.3\% < \varepsilon_\alpha < 16\%$ recorded for an I range of $5.77\% < I < 8.81\%$. Figures 13a and 13b show the TS probe results for test runs with relatively higher I values with relative error range of $8.3\% < \varepsilon_\alpha < 123\%$ recorded for an I range of $6.95\% < I < 18.22\%$.

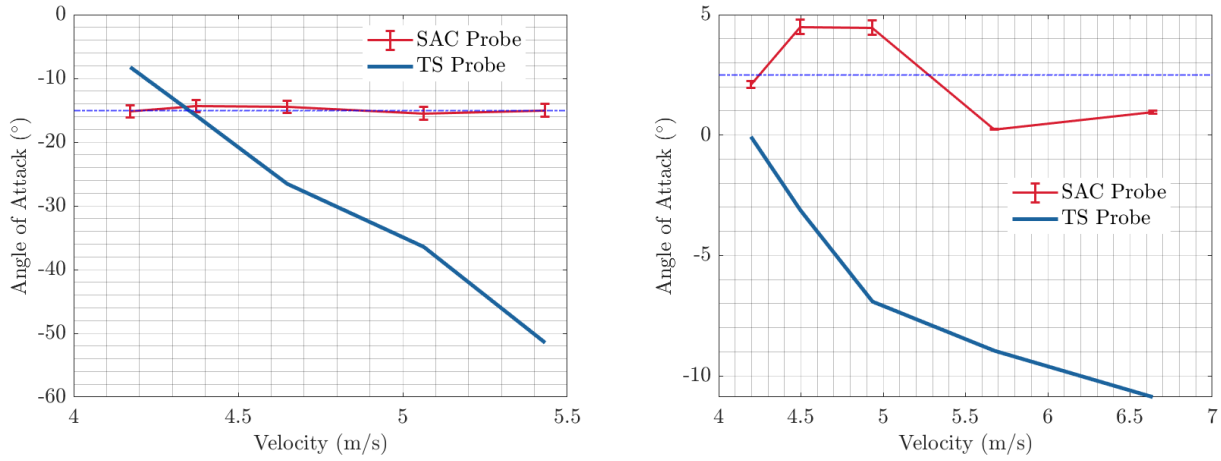


(a) $5.85\% \leq I \leq 8.81\%$



(b) $5.77\% \leq I \leq 7.47\%$

Figure 12 – Comparison between TS and SAC probe results for lower *I* values



(a) $7.53\% \leq I \leq 18.22\%$ (b) $6.95\% \leq I \leq 15.02\%$

Figure 13 – Invalid results for higher *I* data logs

4.3 Frequency Analysis Results

A Butterworth Chebyshev filter was used to try and identify von Karman vortex shedding in the frequency range outlined in Section 3. and in Equation 5. Refer to Table 2 in Appendix B for performance parameters of the filter used. Unfortunately, vortex shedding was unable to be detected. Figure 14 shows a data log for setting $(\alpha^{=} - 7.5°, \beta = 12.5°)$ with the likely vortex shedding frequency range isolated but with no discernible peaks. It is possible this in indicative of high levels of noise within the data with probable causes of this including wind from the roller door of the laboratory being open and the length of the cable from the SAC probe to the UEI cube being long enough to possibly be vulnerable to noise by radiation or conduction.

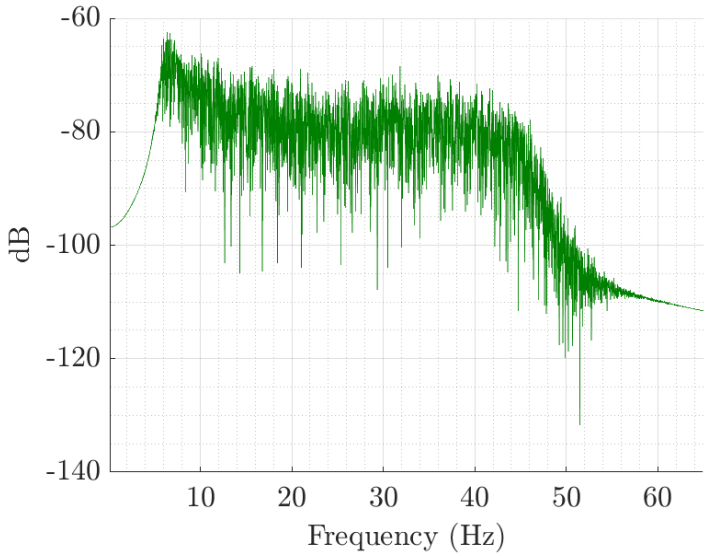
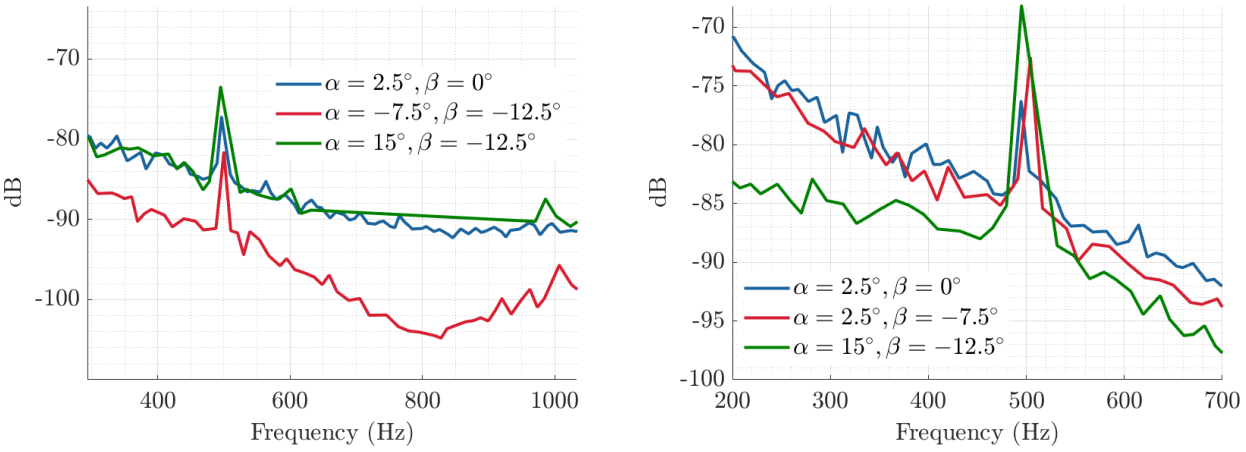


Figure 14 – PSD of dataset following application of filter to try and isolate vortex shedding

However, the frequency analysis did reveal some dominant peaks in the PSD graphs. Looking at the entire frequency axes of derived one-sided PSD graphs, a peak was present across almost every single dataset at $500Hz$, as well as at $1000Hz$ for others. This was identified as the likely structural resonant frequency of the boom. These can be seen in Figure 15



(a) Consistent PSD peaks across all logs (α data) (b) Consistent PSD peaks across all logs (β data)

Figure 15 – Frequency Analysis Results

5. Conclusion

The data acquisition process for the SAC J400 probe has been modernised through the integration of a UEI data acquisition and power supply cube as well as the intergration multi-hole TS probe. Across a series of α, β and v settings, recordings of α were taken from the SAC probe. These recordings had a relative error ranging from $0\% < \varepsilon_\alpha < 25\%$ highlighting sources of systematic and random error ranging from the calibration process of the probe to the use of two static tripods which had to be manually moved for each run test.

Analysis of v data showed great values of I and a strong correlation between I and increasing ε_α from the TS probe was identified. The recorded values of I ranged from $6\% < I < 17\%$ and were larger by a factor of up to 17 than typical values in-flight [5]. This confirmed theory from literature that I values have a great effect on the required calibration factor of multi-hole probes, and therefore on the accuracy of their measurements. This highlighted the error in the experimental setup of the position of the TS probe being outside the centre of the open jet profile of the WindShape.

As can be seen in Figure 16 of Appendix A, the open jet profile of the WindShape only has a limited area of low I. The use of frequency analysis was able to isolate the likely resonant frequency of the boom at $500Hz$, however vortex shedding could not be isolated in the likely frequency range calculated from St formula. Possible causes of this include noise from the analogue signal travelling across the cable and wind from the open roller door.

It should also be noted the University of Sydney has recently acquired a larger WindShape gust tunnel and this should also be considered for future measurements, including use of flow straighteners to improve the flow quality. In future work, dynamic testing should also be considered using this larger gust tunnel. Commissioning has shown spatial and temporal fluctuations of the order of several Hertz are possible. Repeated testing either with this larger gust tunnel, or with a large low-speed wind tunnel would enable the TS probe to not be in an area of high I. A differential pressure sensor and absolute pressure sensor have also been procured to be calibrated and incorporated into the SAC probe for additional v recordings. The setup can also be incorporated into the University's J400 which would enable for further flowfield collection through flight testing and would further aid in the development of a complete Turbulence Suppression system.

6. Contact Author Email Address

The main contact emails for the primary author of this paper is: darren.rajeepan15@gmail.com or darren.rajeepan@sydney.edu.au.
An alternate contact email for the secondary author is nicholas.lawson@sydney.edu.au

7. Copyright Statement

The authors confirm that they, and/or their company or organization, hold copyright on all of the original material included in this paper. The authors also confirm that they have obtained permission, from the copyright holder of any third party material included in this paper, to publish it as part of their paper. The authors confirm that they give permission, or have obtained permission from the copyright holder of this paper, for the publication and distribution of this paper as part of the ICAS proceedings or as individual off-prints from the proceedings.

A WindShape Open Jet Profile and Velocity Variation

Figure 16 below illustrates the variation in velocity across open jet profile of WindShape.

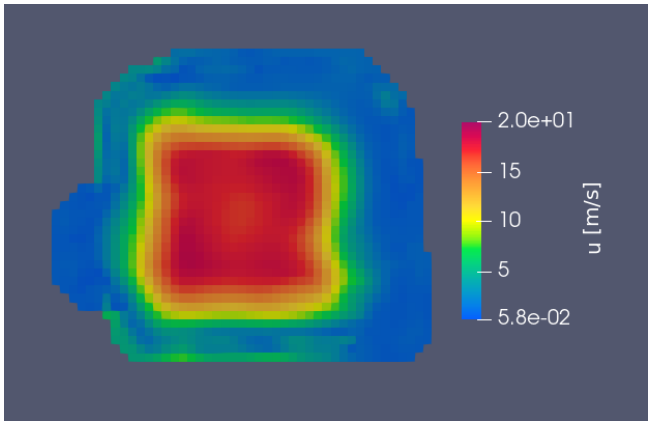


Figure 16 – Velocity variation across WindShape Open Jet Profile (Author: Nishanth Pradyumna)

B Filter Parameters

Table 2 below shows the parameters of the Butterworth Chebyshev IIR digital filter used to try and identify vortex shedding in the likely frequency range identified in Equation 5.

Table 2 – Specifications of Butterworth IIR Band Pass Filter

Stopband Frequency (Hz)		**Passband Frequency (Hz)**		**Stopband Attenuation (dB)**		**Passband Ripple (dB)**	**Sample Rate (Hz)**
Lower	Upper	Lower	Upper	Lower	Uper	1	Adjusted for each log case
4	50	6	44	2	10		

References

[1] Simon Hradecky. Accident: Singapore b773 near bangkok on may 21st 2024, severe turbulence kills one injures 85 passengers. *The Aviaiton Herald*, 2024.

[2] J. Anderson. *Fundamentals of Aerodynamics Sixth Edition*. McGraw Hill Education, 2017.

[3] Warren F. Phillips. *Mechanics of Flight*. JOhn Wiley Sons, 2004.

[4] M. Queisser G. Schitter A. Galffy, N. J. Lawson. Remote flowfield measurements in-flight in a slingsby light aircraft by means of a miniaturised wind lidar. *Applied Aerodynamics Research Conference Royal Aeronautical Society*, 2020.

[5] M. Sitzmann H. Riedel. In-flight investigations of atmospheric turbulence. *Aerospace Science and Technology*, 1998.

[6] M. Moldover C. Crowley, I. Shinder. The effect of turbulence on a multi-hole pitot calibration. *NIST*, 2013.

[7] A. Pope J. B. Barlow, W. H. Rae Jr. *Low Speed Wind Tunnel Testing*. John Wiley Sons, Inc, 1999.

[8] United Electronic Industries. Dnx-ai-217. *User Manual*, 2021.

[9] United Electronic Industries. Dnx-pc-91x. *User Manual*, 2016.

[10] J. F. Foss C. Tropea, A. L. Yarin. *Springer Handbook of Experimental Fluid Mechanics*. Springer, 2007.

[11] H. Eckelmann U. Fey, M. Konig. A new strouhal-reynolds number relationship for the circular cylinder in the range 47<re<2x10e5. *Physics of Fluids*, 1998.

[12] E. R. Keener. Flow-separation patterns on symmetric forebodies. *NASA Technical Memorandum 86016*, 1986.

[13] *Bosch GLL3-80 Professional*.